Earth's rotation perturbation by gravitational waves from compact binaries

Béla Spitalier, Josipa Majstorović, Séverine Rosat

Earth's rotation perturbation by gravitational waves from compact binaries

B. Spitalier*

Université de Strasbourg, CNRS, ITES,

UMR 7063, F-67000 Strasbourg, France

J. Majstorović

Université Paris Cité, Institut de physique du globe de Paris, CNRS, Paris, France,

Now at University of Osijek, Department of Physics, Osijek, Croatia

S. Rosat

Université de Strasbourg, CNRS, ITES,

UMR 7063, F-67000 Strasbourg, France

(Dated: May 12, 2026)

Abstract

Gravitational waves (GWs) are ripples in space-time that propagate deformations caused by compact bodies throughout the universe. As an elastic body, the Earth responds to passing GWs much like a resonant sphere. This interaction produces a redistribution of mass, which results into perturbations of the Earth's tensor of inertia. By conservation of angular momentum, such perturbations lead to a displacement of the rotation axis within the mantle (polar motion) and to changes in the spin rate, directly linked to variations in the length of day (LOD). In this work, we compute for the first time the perturbations of the Earth's rotation induced by GWs emitted by compact white-dwarf binaries, using a normal mode summation approach applied to an elliptical, rotating, radially stratified Earth model. Our results indicate maximal amplitudes of approximately 10^{-15} μs in the LOD and 10^{-15} mas for the polar motion—values that remain far below current instrumental sensitivities. These findings highlight the extreme difficulty of detecting GWs through their rotational effects on the Earth, yet the methodology developed here offers a framework that could be extended to other astrophysical bodies.

INTRODUCTION

The Earth's rotation is known to be non-uniform, with fluctuations arising not only from the gravitational attraction of the Moon, Sun, and other extraterrestrial bodies, but also from mass redistribution at its surface and within its interior [8, 17, 33]. In addition to luni-solar tides, mass changes in the atmosphere, oceans, and hydrosphere (including ice sheet melt), as well as variations in wind patterns and electromagnetic coupling between the Earth's fluid core and the lower mantle, also perturb the Earth's rotation, particularly its axial speed, which is related to the length of day [37]. [7] and [18] have shown that large earthquakes can alter the Earth's tensor of inertia, thereby affecting both the position of the rotation axis and the length of day. Moreover, the

* Contact author: bela.spitalier@etu.unistra.fr

rotation axis itself shifts within the Earth's mantle, a phenomenon known as polar motion.

Gravitational waves (GWs) are ripples in space-time that propagate deformations caused by compact bodies throughout the universe. The Earth, as an elastic body, responds to passing GWs like a resonant sphere. The idea of using the Earth as a giant GW detector was first proposed by Weber [41]. Subsequently, Dyson [15] computed the Earth's response assuming a flat Earth geometry. Predictions of surface deformation induced by GWs were later developed for a spherical Earth by Ben-Menahem [4], and further refined by Coughlin and Harms [9] and Majstorović et al. [29, 30], the latter using a more realistic model of the Earth as a rotating, ellipsoidal 3D body. Moreover, several studies have investigated how GWs excite vibrations in spheres [1, 23], elastic solids [13, 14], stars [6, 21, 24–26, 32, 35, 36, 40], and the Moon [5, 20, 22, 31, 43].

Surface deformation associated with the Earth's resonant response to gravitational waves (GWs) perturbs its tensor of inertia due to the resulting mass redistribution. By conservation of angular momentum, a perturbation in the tensor of inertia must be compensated by a change in the Earth's instantaneous rotation vector. This principle is based on the same equations used by Chao and Gross [7] to describe the effects of earthquakes, except that here we consider the mass redistribution caused by GW-induced surface deformation. A previous study has computed the perturbation of the Earth's rotation by GWs [34], however, their approach relied on a static gravitational field approximation, which is not valid in the context of GWs whose frequencies can greatly exceed the Earth's rotation rate, as is the case, for instance, with massive binary systems such as white-dwarf binaries.

In this work, we compute for the first time the perturbation of the Earth's rotation by gravitational waves (GWs) using a normal mode summation approach, similar to that employed in Majstorović et al. [29]. First, we develop the equations used to calculate the perturbations of the Earth's tensor of inertia and gravitational field. We then quantify the effects for GWs emitted by selected white-dwarf binary systems. The resulting perturbations in the length of day and polar motion are compared with known geophysical effects on the Earth's rotation, as well as with the precision of current

geodetic instruments used to measure these variations. Finally, we provide discussion, conclusions, and perspectives for future work.

I. METHOD

The primary objective of this study is to develop an indirect method for detecting gravitational waves (GWs), using the Earth itself as a sensing instrument. We model the Earth as an elastic, rotating body in space. In contrast to previous studies that focused on GW-induced deformations of the Earth [4, 15, 29], our approach investigates the rotational perturbations resulting from such deformations. The methodology is outlined below. We begin by quantifying the Earth's rotational (Subsection 1.1) and gravitational (Section 1.2) perturbations induced by mass redistribution, following the formulations of [7, 18]. Section 1.3 presents the displacement field induced by GWs from white-dwarf binaries, modeled for a rotating, anelastic, radially heterogeneous Earth. Finally, in Section 1.4, we derive, for the first time, analytical expressions for the perturbation of the Earth's gravitational field.

A. Density field perturbation

We can express mass redistributions within the Earth in terms of variations of the multipole moments of the density field [7, 18]. When normalized, these coefficients are refered Stokes coefficients of degree l and order m C_{lm} and S_{lm}, typically denoted as C_{lm} and S_{lm}, such that

$$C_{lm} + iS_{lm} = \frac{N_{lm}}{Ma^l} \int_{V_0} r^l Y_{lm}(\theta, \phi) \rho(\mathbf{r}) dV, \tag{1}$$

where N_{lm} are normalization factors relative to the normalization of the spherical harmonics $Y_{lm}(\theta, \phi)$, a is the Earth radius, M is the Earth mass and V_0 is the Earth volume. All the necessary constants and variables are summarized in tables I and II. Here we use the same normalized spherical harmonics $Y_{lm}(\theta, \phi)$ as in [29] and written

in their complete form in appendix A. Introducing a small deformation of the Earth, where a mass dm is displaced from the position $\mathbf{r}$ to $\mathbf{r}+\mathbf{u}$, with $\|\mathbf{u}\| \ll \|\mathbf{r}\|$,leads to the following perturbation of the Stokes coefficients

$$\Delta C_{lm} + i\Delta S_{lm} = \frac{N_{lm}}{Ma^l}\int_{V_0} r^{l-1}\mathbf{u}\bullet(\hat{\mathbf{r}}l + \nabla_h)Y_{lm}(\theta,\phi)\rho(\mathbf{r})dV, \tag{2}$$

where ∇_h is the surface gradient [10] and $\bullet$ denotes the dyadic product of two tensors.

Although Stokes coefficients characterize the Earth's gravity field and do not directly describe its rotation, they can be incorporated into the equations governing polar motion and variations in the length of day, quantities that we use to study the rotational response of the Earth. It is the topic of the next subsection.

B. Rotation perturbation

The Earth's rotation varies over time. These variations are characterized by the varying spatial motion of a conventional axis, which remains close to the true instantaneous rotation axis. The movements of this axis, as observed in a terrestrial reference frame attached to the Earth's mantle, is referred to as polar motion. The same motions, when viewed in a celestial reference frame, corresponds to precession and nutation. The intersection between this conventional axis with the Earth's surface defines the Celestial Intermediate Pole (CIP). Polar motion is thus defined as the movement of the CIP, whose coordinates in the International Terrestrial Reference Frame (ITRF) are denoted by (x_p, y_p).

Developing the theorem of the conservation of angular momentum for an ellipsoidal rotating Earth leads to a system of equations known as the *Euler-Liouville equations* Munk and Macdonald [33]. Here we consider a biaxial Earth model. In absence of external torque, the linearized Liouville equations are then written

$$p + \frac{i}{\sigma_e}\dot{p} - \frac{i}{\Omega}\frac{d}{dt}\left(p + \frac{i}{\sigma_e}\dot{p}\right) = \frac{c}{C-A} + \frac{h}{(C-A)\Omega} - \frac{i}{\Omega}\left(\frac{\dot{c}}{C-A} + \frac{\dot{h}}{(C-A)\Omega}\right), \tag{3}$$

where we have introduced the complex notation $p = x_p - iy_p$. A and C are the Earth's main inertia moment, Ω is the mean angular velocity of the Earth (Ω =

$7.292115 \cdot 10^{-5}$ rad/s). σ_e is the Euler pulsation related to the Earth's flattening as $\sigma_e = \frac{C-A}{A}\Omega$ corresponding to a period of 303.6 solar days. h are the changing equatorial components of the angular momentum usually associated with the motion of fluids like the atmosphere (winds). c are the changes in the main equatorial inertia moments ($c = \Delta I_{xx} + i\Delta I_{zz}$). We write χ the polar motion excitation function corresponding to the term on the right-hand side of Eq. (3) as

$$\chi = \chi_x + i\chi_y = \frac{c}{C-A} + \frac{h}{(C-A)\Omega} - \frac{i}{\Omega}\left(\frac{\dot{c}}{C-A} + \frac{\dot{h}}{(C-A)\Omega}\right). \tag{4}$$

In short this polar motion function describes the motion of the rotational axis relatively to the crust. We can see that $\chi_y = \dot{\chi}_x$ and therefore we have

$$p + \frac{i}{\sigma_e}\dot{p} - \frac{i}{\Omega}\frac{d}{dt}\left(p + \frac{i}{\sigma_e}\dot{p}\right) = \chi_x + i\dot{\chi}_x. \tag{5}$$

In order to take into account the core decoupling and the effect of the Earth non-rigidity [2, 18, 39] we usually add two numerical factors (1.61 and 1.44, respectively) into Eq. (5) as

$$\chi_x = \frac{1.61}{\Omega(C-A)}\left[h(t) + \frac{\Omega \mathbf{c}(t)}{1.44}\right]. \tag{6}$$

If we assume that the source is not loading the Earth and occurs instantaneously, which means that they have no relative angular momentum ($h = 0$), there will be a perturbation on the inertia momenta leading to the following polar motion excitation function [18]

$$\Delta\chi_{eq} = \frac{1.61}{\Omega(C-A)}(\Delta I_{xz} + i\Delta I_{yz}). \tag{7}$$

According to MacCullagh theorem ([33]), there is a simple relation between the degree-2 Stokes coefficients, introduced in section I A and the elements of the tensor of inertia

$$\begin{aligned} I_{xz} &= -\sqrt{\frac{5}{3}}Ma^2C_{21}, \\ I_{yz} &= -\sqrt{\frac{5}{3}}Ma^2S_{21}, \\ I_{zz} &= \frac{1}{3}\left[T - \sqrt{20}Ma^2C_{20}\right], \end{aligned} \tag{8}$$

with T being the trace of the inertia tensor ($T = I_{xx} + I_{yy} + I_{zz}$). We can now express the perturbation of the polar axis coordinates using the variation of Stokes coefficients that was introduced in Eq. (2) as

$$\Delta\chi_{eq} = -\sqrt{\frac{5}{3}}\frac{1.61}{\Omega(C-A)}Ma^2(\Delta C_{21} + i\Delta S_{21}). \tag{9}$$

Polar motion is our first parameter to study Earth rotation. Besides, the conservation of the angular momentum imposes that a variation in the third component (z-axis) of the Earth's inertia tensor will induce a variation in Earth's angular velocity, which is also a variation in the length of day (LOD). We can express the variation in the LOD ($\Delta\Lambda(t)$) induced by a deformation as

$$\Delta\Lambda(t) = \frac{\Lambda_0}{C_m}\Delta I_{zz}(t), \tag{10}$$

with Λ_0 the nominal length of day (86,400 s) and C_m the polar momentum of inertia of the Earth's crust and mantle. Then, using the relation between I_{zz} and C_{20} from Eq. (8) we find

$$\Delta\Lambda(t) = \frac{1}{3}\frac{\Lambda_0}{C_m}[\Delta T - \sqrt{20}Ma^2\Delta C_{20}]. \tag{11}$$

$\Delta\Lambda$ varies with ΔC_{20}, given by Eq. (2), and with the trace of the inertia tensor defined as

$$T = 2\int_{V_0} r^2\rho(\mathbf{r})dV. \tag{12}$$

By expanding the previous integrand in a Taylor series, the variation in the trace of the inertia tensor is written

$$\Delta T = 4\int_{V_0} \mathbf{r}\cdot\mathbf{u}(\mathbf{r},t)\rho(\mathbf{r})dV. \tag{13}$$

We summarize the previously introduced variables and constants, in the tables I and II respectively. Since the trace of the inertia tensor in Eq. (13) depends on the induced displacement $\mathbf{u}$, in the next chapters we shall assume that this deformation is caused by the passing GWs. Next, using equations (2), (9) and (11), we can find the gravitational and rotational perturbations, respectively. This requires a knowledge of the surface deformation due to GWs, which we introduce in the next section.

Variables	Symbol	Definition
Inertia tensor	I	$\begin{bmatrix} A & 0 & 0 \\ 0 & A & 0 \\ 0 & 0 & C \end{bmatrix}$
Perturbed inertia tensor	ΔI	$\begin{bmatrix} A+c_{11} & c_{12} & c_{13} \\ c_{21} & A+c_{22} & c_{23} \\ c_{31} & c_{32} & C+c_{33} \end{bmatrix}$
Trace of inertia tensor	$T = \sum_i I_{ii}$	$2\int_{V_0} r^2 \rho(\mathbf{r}) dV$
Stokes coefficients	C_{lm} and S_{lm}	$C_{lm} + iS_{lm} = \frac{N_{lm}}{Ma^l}\int_{V_0} r^l Y_{lm}(\theta,\phi)\rho(\mathbf{r})dV$
Perturbed Stokes coefficients	ΔC_{lm} and ΔS_{lm}	$\frac{N_{lm}}{Ma^l}\int_{V_0} r^{l-1}\mathbf{u}\cdot(\hat{\mathbf{r}}l + \nabla_h)Y_{lm}(\theta,\phi)\rho(\mathbf{r})dV$
Polar motion	$\Delta\chi_{eq}$	$-\sqrt{\frac{5}{3}}\frac{1.61}{\Omega(C-A)}Ma^2(\Delta C_{21} + i\Delta S_{21})$
Variation in the LOD	$\Delta\Lambda(t)$	$\Delta\Lambda(t) = \frac{\Lambda_0}{C_m}\Delta I_{zz}(t)$

TABLE I. Summary of the most important variables used in sections I A and I B

Constant	Symbol	Value
Earth's mean radius	a	6.371 10^6 m
Earth's mass	M	5.9722 10^{24} kg
Principal inertial momentum	A	8.0101 10^{37} kg.m^2
Axial inertial momentum	C	8.0365 10^{37} kg.m^2
Earth's mean angular velocity	Ω	7.292115 10^{-5} rad/s

TABLE II. Summary of the most important constants used in sections I A and I B

C. Gravitational wave perturbations

Following work of [4, 28, 29], we adopt a normal-mode summation approach to derive an analytical solution for the Earth's response to incoming GWs. First, we solve the equation of motion without external forcing. Then, this free-source solution is contracted with the GW force to obtain the displacement induced by GWs. The solution of the free-source equation is represented by a Green tensor, $\mathbf{G}(\mathbf{x}, \mathbf{x}'; \mathbf{t} - \mathbf{t}')$,

which describes the displacement at position $\{\mathbf{x}, t\}$ due to an impulse point force at position $\{\mathbf{x}', t'\}$. This expression depends solely on the body for which we are solving the equation of motion. Using the Green tensor, we can define the displacement from equilibrium as

$$\mathbf{u}(\mathbf{r}, t) = \int_{-\infty}^{t} \int_{V} \mathbf{G}(\mathbf{r}, \mathbf{r}'; t-t') \cdot \mathbf{f}(\mathbf{r}', t') dV' dt' + \int_{-\infty}^{t} \int_{S} \mathbf{G}(\mathbf{r}, \mathbf{r}'; t-t') \cdot \mathbf{t}(\mathbf{r}', t') d\Sigma' dt', \quad (14)$$

where $\mathbf{f}(\mathbf{r}', t')$ and $\mathbf{t}(\mathbf{r}', t')$ are volumetric and surface forces, respectively, which depend on the source of the excitations, i.e. here a GW source.

To obtain an analytical solution of Eq. (14), we need to adopt a specific set of approximations related to the Green tensor as well as the GW force. Regarding the Green tensor, we adopt a solution for an anelastic, radially heterogeneous Earth model, where rotation and lateral variations are considered only in the context of eigenfrequency perturbations. Regarding the external force, we assume that GWs encountering Earth are weak, meaning that space-time has no curvature far from any significant mass. Thus, we adopt a flat-space approximation, where we decompose the gravitational metric into the Minkowski metric and a small perturbation $h_{\mu\nu}$, by assuming $|h_{\mu\nu}| \leq 1$. This further implies that we can treat GWs in a non-relativistic framework where GWs can be considered as plane waves in a three dimensional Euclidean space. It has been shown that in the flat-space approximation, the definition of the GW force depends on the observational framework one adopts [1, 3, 27, 31]. If one aims to measure the direct strain generated by the GW force on an elastic medium, the appropriate approach is to adopt a Newtonian tidal force term. However, if the goal is to measure the relative displacement of the Earth's surface with respect to the Earth's center of mass using a free-fall mass—as is done by a seismometer—then the force should be defined by

$$\mathbf{f}(\mathbf{r}, t) = \frac{\partial \mu}{\partial r} \hat{e}_r \cdot \mathbf{h}(\mathbf{r}), \quad (15)$$

where μ is the shear modulus, $\hat{e}_r$ is the unit vector in radial direction and $\mathbf{h}$ is a metric perturbation [1, 15, 31]. Since our framework involves a term related to relative displacement (see Eq. 2 and Eq. 13), we adopt the former. We emphasize that both formulations of the force term are valid within their respective mathematical

frameworks. The choice between them depends on the specific physical problem under consideration, particularly its relevant frequency range, or on the design requirements of the instrument, as discussed in the literature [1, 3, 27, 31, 43]. The retained definition of the GW force implies that GWs only interact with the variations of the shear modulus μ inside an elastic medium. For the Earth, there are two major discontinuities in the shear modulus profile: at the free surface and at the core-mantle boundary (CMB). In essence, by this definition, the Earth can be considered to be constantly affected by the force term from Eq. (15). Further, to take into account a specific source of GWs, such as the white-dwarf or neutron star binaries, we need to introduce some binary parameters into the definition of the metric perturbation $\mathbf{h}(\mathbf{r})$, which will follow in the next subchapter.

Eventually, we also need to consider the reference frame in which we want to make the measurement with respect to the reference frame where the source is positioned. Clearly, we want to carry out the measurement in the Terrestrial Reference Frame, while the source is naturally defined in the Celestial Reference Frame. To properly account for this, we need a rotation matrix that transforms unit vectors from the Celestial to the Terrestrial Reference Frame, which can be found in Appendix B.

1. Metric perturbation by white-dwarf binaries

Considering that GWs have a double polarization, which is conventionally represented as "+" and "×", we can write the metric perturbation as

$$\mathbf{h} = h_+ e_+ + h_\times e_\times, \tag{16}$$

where h_+ and $h_\times$ are time functions related to each polarization of the GWs and e_+ and $e_\times$ are polarization tensors for plane-waves in a three dimensional Euclidean space defined as

$$e_+ = \begin{bmatrix} 1 & 0 & 0 \\ 0 & -1 & 0 \\ 0 & 0 & 0 \end{bmatrix} \quad \text{and} \quad e_\times = \begin{bmatrix} 0 & 1 & 0 \\ 1 & 0 & 0 \\ 0 & 0 & 0 \end{bmatrix} \tag{17}$$

The time functions depend on the source, thus if we consider a white-dwarf binary system, we can define them as

$$\begin{aligned} h_+ &= h_{+,c}\cos(2\Omega_{GW}t), \\ h_\times &= h_{\times,c}\sin(2\Omega_{GW}t), \end{aligned} \tag{18}$$

where the constant amplitudes $h_{+,c}$ and $h_{\times,c}$ are

$$\begin{aligned} h_{+,c} &= -2(1+\cos^2\iota)\frac{G}{c^4}\frac{\mu_r a^2\Omega_{GW}^2}{r}, \\ h_{\times,c} &= -4\cos\iota\frac{G}{c^4}\frac{\mu_r a^2\Omega_{GW}^2}{r}, \end{aligned} \tag{19}$$

with the binary parameters defined as follows: ι is the inclination angle between the normal to the orbit and the line of sight, Ω_{GW} is the orbital frequency of the source, c is the speed of light in a vacuum ($299,792,458$ m/s), G is the gravitational constant (6.67408×10^{-11} m^{3}kg^{-1}s^{-2}), r is the distance from the source, μ_r is the reduced mass of the system, and a is the distance between the two stars. The amplitudes can be calculated for each detected binary star system, as shown in [28], and vary between 10^{-23} and 5×10^{-22}. In the millihertz frequency regime, these sources persist in time. Due to this consistency, we consider these sources to be monochromatic and represent them using simple cosine and sine time functions, as shown in Eq. (18).

2. Induced Earth's response due to gravitational waves

By solving the contraction in Eq. (14) between the Green's tensor and the GW force term given in Eq. (15), arising from white-dwarf binaries, we obtain the Earth's induced response. This solution consists of several components. First, the geometrical pattern, expressed by $f^m_{+,\times}(\gamma(t),\alpha,\delta,\psi)$, indicates the combinations of incident angles that yield the strongest response for both polarizations (+ and ×). Second, the source time function $\bar{g}_{+,\times}(t,\Omega,\omega_k)$, which encodes the frequency dependence of the solution. Third, the eigenfunctions $\hat{s}_k$. And fourth, the model functions $\zeta_k(r)$, whose definitions are provided in Appendix C and in Majstorović et al. [29]. The displacement for mode

is hence written as

$$u_k(\mathbf{r},t) = \hat{s}_k(\mathbf{r})\delta_{l,2}\big[h_{+,c}\bar{g}_+(t,\Omega_{GW},\omega_k)f_+^m(\gamma(t),\alpha,\delta,\psi)+h_{\times,c}\bar{g}_\times(t,\Omega_{GW},\omega_k)f_\times^m(\gamma(t),\alpha,\delta,\psi)\big]\zeta_k(r), \tag{20}$$

where k stands for collective set of indices $\{n,l,m\}$ with n being the overtone index designating the radial order of the eigenfrequencies, l the angular degree, and m the azimuthal order within the normal mode convention. Definitions of other functions are given in Appendix C. As previously noted, only the $l=2$ degree modes are excited due to the contraction between the spherical Earth and the double polarization of the GWs [29].

D. Perturbation of the Earth's gravitational field

Equations (9) and (13) are solved by injecting the displacement u_k from Eq. (20) in place of $\mathbf{u}$. The resulting integrals can be partially solved after computing the the dyadic products from $\mathbf{s}_k(\mathbf{r},t)\bullet(\hat{\mathbf{r}}l+\nabla_h)Y_{2m}(\theta,\phi)$ and $\mathbf{r}\bullet\mathbf{s}_k(\mathbf{r},t)$. We define two integrals $R_1(t)$ and $R_2(t)$ as

$$\Delta C_{lm} + i\Delta S_{lm} = \frac{N_{lm}}{Ma^2}R_{1,lm}, \tag{21}$$

$$\Delta T = 4R_2(t), \tag{22}$$

$$R_1(t) = \int_{V_0} r^{l-1}\sum_{n'} u_k(\mathbf{r},t)\bullet(\hat{\mathbf{r}}l+\nabla_h)Y_{lm}(\theta,\phi)\rho(\mathbf{r})dV, \tag{23}$$

$$R_2(t) = \int_{V_0} \mathbf{r}\sum_{k'}\bullet u_{k'}(\mathbf{r},t)\rho(\mathbf{r})dV. \tag{24}$$

We also define $R_{1,lm}(t)$ for a given order l and degree m ($R_1(t) = \sum_{l',m'} R_{1,l'm'}(t)$).

By linearity of the dyadic product, Eq. 23 and 24 can be decomposed into a sum of nine and three dyadics, respectively, which leads to a respective sum of nine and three integrals. Once the dyadics have been computed, no simple expression can be obtained for the integral $R_{1,lm}$.

We start with only one mode, which means we compute $R_{2,k}$ (with k being a given mode (n,l,m). And since only $l=2$ Earth's normal modes interact with GWs, thus we

have $(k:(n,2,m))$. We can separate the displacement into three parts by considering the radial, longitudinal and latitudinal dependencies of the eigenfunction as shown here

$$u_k(\mathbf{r},t) = u_r(\mathbf{r})Y_{2m}(\theta,\phi)\hat{e}_r + u_\theta(\mathbf{r})\kappa^{-1}\partial_\theta Y_{2m}(\theta,\phi)\hat{e}_\theta + u_\phi(\mathbf{r})\kappa^{-1}\frac{1}{\sin\theta}\partial_\phi Y_{2m}(\theta,\phi)\hat{e}_\phi, \quad (25)$$

where $(\hat{e}_r,\hat{e}_\theta,\hat{e}_\phi)$ are the unit vectors of the spherical coordinate system (see Appendix D) and (u_r,u_θ,u_ϕ) are the radial eigenfunctions defined in Appendix C. Next, we apply a factorization which leads to

$$R_{2,k}(t) = \left[\frac{1}{3}\int_0^a r^3\rho(r)u_r^r(r)dr + \kappa^{-1}\int_0^a r^3\rho(r)u_\theta^r(r)dr\right]I_2, \quad (26)$$

with $I_2 = 3\delta_{l,2}I_1$, I_1 from Appendix C and $u_r^r(r)$ and $u_\theta^r(r)$ the radial parts of the displacement, for an order m. They are defined by

$$\begin{aligned} u_r^r(r) &= {}_nU_2(r)\,{}_n\zeta_2(r)\Gamma_{+,\times}^m, \\ u_\theta^r(r) &= \kappa^{-1}\,{}_nV_2(r)\,{}_n\zeta_2(r)\Gamma_{+,\times}^m, \\ \Gamma_{+,\times}^m &= h_{+,c}\bar{g}_+(t,\Omega_{GW},\omega_0)f_+^m(\gamma(t),\alpha,\delta,\psi) + h_{\times,c}\bar{g}_\times(t,\Omega_{GW},\omega_0)f_\times^m(\gamma(t),\alpha,\delta,\psi). \end{aligned} \quad (27)$$

The longitudinal and latitudinal integrals can be analytically solved, while the integrals depending on r shall be solved numerically. In fact, the radial integrals involve the density function $\rho(r)$, which is not analytically integrable.

At this point, we need to modify the pattern function $f_{+,\times}^m(\gamma(t),\alpha,\delta,\psi)$ used in [29] and included in the definition of s_r^r and s_θ^r. These functions describe the pattern of the localized Earth's response to a perturbation. Here we look at the global response of the Earth (in terms of rotational perturbation) to the same kind of perturbation. Thus we should update these functions by including the factorized I_2 matrix such as

$$\begin{aligned} f_{I,+}^m(\gamma(t),\alpha,\delta,\psi) &= e_+ : \left\{\frac{1}{9}I_2 * I_2\right\}, \\ f_{I,\times}^m(\gamma(t),\alpha,\delta,\psi) &= e_\times : \left\{\frac{1}{9}I_2 * I_2\right\}. \end{aligned} \quad (28)$$

It is important to keep the order of computation (matrix product before contraction) so that the geometrical information contained in the mathematical tensor $R_{2,k}$ is preserved. Using this definition of $f_{+,\times}^m(\gamma(t),\alpha,\delta,\psi)$, Eq. 26 and the definition of the eigenfunctions

(Appendix C), we can write $R_2(t)$ as

$$R_2(t) = \sum_{n'} \sum_{m'} \Big[\int_0^a r^3 \rho(r)\, {}_{n'}U_2(r)\, {}_{n'}\zeta_2(r) dr + 3\kappa^{-1} \int_0^a r^3 \rho(r)\, {}_{n'}V_2(r)\, {}_{n'}\zeta_2(r) dr \Big] \Gamma^{m'}_{+,\times}. \tag{29}$$

Next, we use a trapezoidal rule to find numerical approximations of the remaining integrals related to the radial dependencies. In summary, to determine $R_2(t)$, we separate the different dependencies in $u_k(\mathbf{r}, t)$, we solve the integrals related to θ and ϕ, we also determine the new pattern functions and finally, we compute the radial integrals by a numerical approach. The same routine can be used to determine $R_{1,lm}$. However, an important difference should be taken into account after the computation of the dyadics. Indeed we have

$$\begin{aligned}
&u_k(r,t) \bullet (2\hat{e}_r + \nabla_h) Y_{2m}(\theta,\phi) \\
&\qquad = 2u_r^r(r) Y_{2m}(\theta,\phi) \hat{e}_r \bullet \hat{e}_r + u_r^r(r) \partial_\theta Y_{2m}(\theta,\phi) \hat{e}_r \bullet \hat{e}_\theta + \frac{u_r^r(r)}{\sin\theta} \partial_\phi Y_{2m}(\theta,\phi) \hat{e}_r \bullet \hat{e}_\phi \\
&\qquad + 2u_\theta^r(r) Y_{2m}(\theta,\phi) \hat{e}_\theta \bullet \hat{e}_r + u_\theta^r(r) \partial_\theta Y_{2m}(\theta,\phi) \hat{e}_\theta \bullet \hat{e}_\theta + \frac{u_\theta^r(r)}{\sin\theta} \partial_\phi Y_{2m}(\theta,\phi) \hat{e}_\theta \bullet \hat{e}_\phi \\
&\qquad + 2u_\phi^r(r) Y_{2m}(\theta,\phi) \hat{e}_\phi \bullet \hat{e}_r + u_\phi^r(r) \partial_\theta Y_{2m}(\theta,\phi) \hat{e}_\phi \bullet \hat{e}_\theta + \frac{u_\phi^r(r)}{\sin\theta} \partial_\phi Y_{2m}(\theta,\phi) \hat{e}_\phi \bullet \hat{e}_\phi
\end{aligned} \tag{30}$$

with $u_\phi^r = u_\theta^r$. Once each dyadic has been solved, there is no common factor between the nine terms of Eq. (30). Thus, it is not possible to use a common new set of pattern functions. However, we still need to include the results of the dyadics (a second order tensor) in the contraction (as we did in Eq. (28)). Instead of a common set of functions $f^m_{I,+,\times}$, we use nine new pattern functions $f^{m*}_{I,+,\times}$ which correspond to the nine dyadics. Eventually, we can show that

$$R_{1,lm} \propto \int_0^a \rho(r) r^3 \begin{vmatrix} u_r^r(r) \\ u_\theta^r(r) \end{vmatrix} dr, \begin{vmatrix} \delta_{m,1} \\ \delta_{m,0} \\ \delta_{m,-1} \end{vmatrix} \delta_{l,2}, \tag{31}$$

with δ_{xm} the Kronecker symbol equal to one when $m = x$ and equal to zero otherwise.

Here we use a slightly different definition of $u_r^r(r)$ and $u_\theta^r(r)$

$$\begin{aligned} u_r^r(r) &= {}_nU_2(r)\ {}_n\zeta_2(r)\Gamma_{+,\times}^{m,*}, \\ u_\theta^r(r) &= \kappa^{-1}\ {}_nV_2(r)\ {}_n\zeta_2(r)\Gamma_{+,\times}^{m,*}, \\ \Gamma_{+,\times}^{m,*} &= h_{+,c}\bar{g}_+(t,\Omega,\omega_0)f_+^m(\gamma(t),\alpha,\delta,\psi)^* + h_{\times,c}\bar{g}_\times(t,\Omega,\omega_0)f_\times^m(\gamma(t),\alpha,\delta,\psi)^*, \end{aligned} \tag{32}$$

which includes the new pattern functions.

II. RESULTS

As a first result of this study, we note the loss of orders -2 and 2 in equations describing the gravitational perturbation (see Eq. (31 and Eq. (21)). The loss of all degrees except degree two originates from the equation of the surface displacement provided by [29] and is due to the traceless and symmetric properties of general relativity tensor h ([27], [29]). Mathematically, loss of orders -2 and 2 is explained by the double projection of spherical harmonics in the computation of geometrical functions (see appendix C) and in Eq. (2).

Moreover, we solved the equations of LOD and polar motion variations using the integrals $R_1(t)$ and $R_2(t)$ derived in previous sections. It leads us to these new expressions

$$\Delta C_{lm} + i\Delta S_{lm} = \frac{N_{lm}}{Ma^2}R_{1,lm}(t), \tag{33}$$

$$\Delta T = 4R_2(t). \tag{34}$$

Then, with Eq. (9) and (11) we have

$$\Delta\chi_{eq}(t) = -\sqrt{\frac{5}{3}}\frac{1.61}{\Omega(C-A)}N_{lm}R_{1,21}(t), \tag{35}$$

$$\Delta\Lambda_{eq}(t) = \frac{1}{3}\frac{\Lambda_0}{C_m}[4R_2(t) - \sqrt{20}N_{lm}R_{1,20}(t)]. \tag{36}$$

More precisely, we should use the real part of R_1 ($\mathbb{R}(R_{1,20}(t))$) instead of $R_{1,20}(t)$ in Eq. (36). However, there is no imaginary part when $m = 0$, which means $\mathbb{R}(R_{1,20}(t)) = R_{1,20}(t)$.

From the previous development, we can conclude that the results depend on both time t and the star, described by its position angles $\gamma(t)$, α and δ and the amplitudes of the metric perturbation h_+ and $h_\times$ (see section I C 1). Indeed, the relative position of the star with respect to the Earth is changing with time, thus the pattern functions are time dependent.

Figure 1 shows the time variations of the perturbation of the LOD for the binary star system SDSS J0651+2844 (see table III). It is a very weak periodic signal whose order of magnitude is $10^{-17}\mu$s. A change in the value of the polarization angle induces

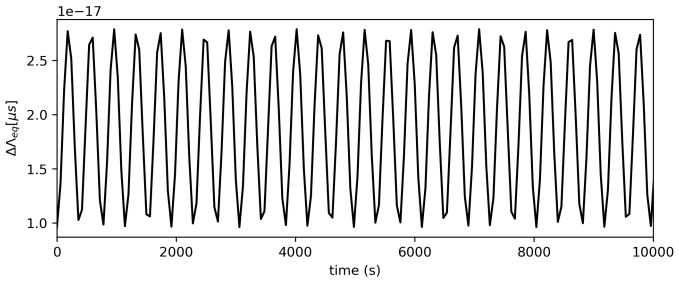

FIG. 1. Time dependency of the LOD variations induced by GWs from the star system SDSS J0651+2844 with a rotation angle $\psi = 0°$.

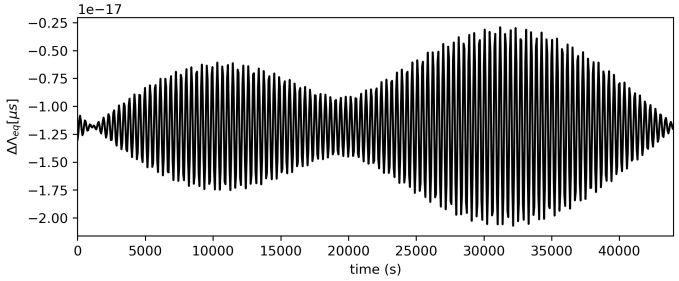

FIG. 2. Time dependency of the LOD variations induced by GWs from the star system SDSS J0651+2844 with a rotation angle $\psi = 40°$.

a modulation of the signal, which is illustrated in Figure 2. We also see a decrease by one order of magnitude.

In order to compare these perturbations with other environmental or geophysical effects occurring on Earth, we have computed the Amplitude Spectral Densities (ASD), either in $\mu s \cdot \mathrm{Hz}^{-1/2}$ for the LOD or in $\mathrm{mas} \cdot \mathrm{Hz}^{-1/2}$ for the polar motion.

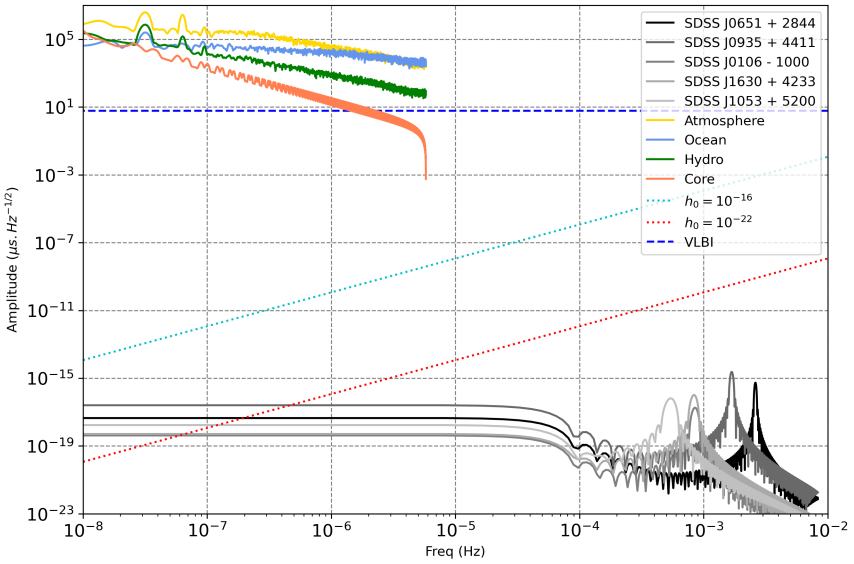

FIG. 3. Amplitude spectral densities of the length of day variations induced by GWs emitted from five different star systems (in black and gray colors) during one day of observation. The GW-origin LOD variations are compared with the effects of atmospheric, oceanic, hydrological mass redistributions and core angular momentum transfer as modeled on Earth. The sensibility limit of the VLBI technique is plotted in horizontal dashed line. The estimation from [34] (with GWs of respective amplitudes 10^{-16} and 10^{-22}) are represented by the oblique dotted lines. The strain amplitudes of the GWs for the five star systems are between 10^{-23} and 5×10^{-22}.

Figure 3 shows the ASD of the LOD associated to five binary star systems compared with the effects of the superficial fluid layers (atmosphere, ocean and hydrology) and of the core. GW-induced perturbations are simulated over one day with a sampling rate of one minute. The amplitude peaks lie in between 10^{-16} and 10^{-14} μs, which is significantly lower than the amplitude of the other effects (ranging from 10 and 10^5 μs).

The detectability range of the VLBI (around 10 μs) is used as a benchmark for the current instrumental capacities. Additionally, we compare with the previous study [34], which proposed another approach to model the interaction between GWs and Earth's rotation. It uses a specific choice of coordinates asymptotically Cartesian and mass-centered ([19, 38]), usually applied to the study of stars ([11, 19]). Considering

a spherically symmetric body of mass M and a GW associated with an external static tidal field, one can show that the body will develop a quadrupole moment Q_{ij} in response to the tidal tensor E_{ij} with

$$Q_{ij} = -\frac{2}{3} k_2 \frac{a^5}{G} E_{ij}. \tag{37}$$

With k_2 the degree-2 Love number and E_{ij} is related to the GW amplitude, in the TT gauge, by $E_{ij} = \omega_g^2 / 2 h_{ij}^{TT}$, where ω_g denotes the GW frequency. Note, the ω_g^2 dependency of the perturbation. The quadrupole is interpreted as the perturbation of the inertia tensor I_{ij}

$$I_{ij} = \begin{bmatrix} A + c_{11} & c_{12} & c_{13} \\ c_{21} & A + c_{22} & c_{23} \\ c_{31} & c_{32} & C + c_{33} \end{bmatrix}_{ij}, \tag{38}$$

$$Q_{ij} = -c_{ij}. \tag{39}$$

Thus it is possible to compute the induced variation in the Earth's rotation. Note that this quadrupole approach models the direct interaction between the GW and the Earth's inertia tensor, thus there is no amplification with the seismic normal modes. The used approximations are valid at low frequencies ($f_{GW} \ll 10^{-3}$ mHz) but were extrapolated to higher frequencies to provide an order of magnitude of the expected results (see Figure 3). Because they have an amplitude proportional to ω_g^2, the LOD and polar motions perturbations are strictly increasing and are several orders of magnitude higher than our results. We note that these should be regarded as first-order extrapolations, and that, since the phenomena examined in [34] lie in the very low-frequency regime, the frequency range associated with the Earth's normal modes is the most relevant for our analysis.

Similarly, Figure 4 shows the ASD of the GW-induced polar motion for the five same star systems and compared with the effects of atmosphere, ocean and hydrology. The core does not appear as it has no effect on the polar motion. The variations of polar motion are around 10^{-18} mas. At the pole, 1 mas is equivalent to a 3-cm displacement, which means that the movements of the pole induced by GWs of this amplitude are currently undetectable.

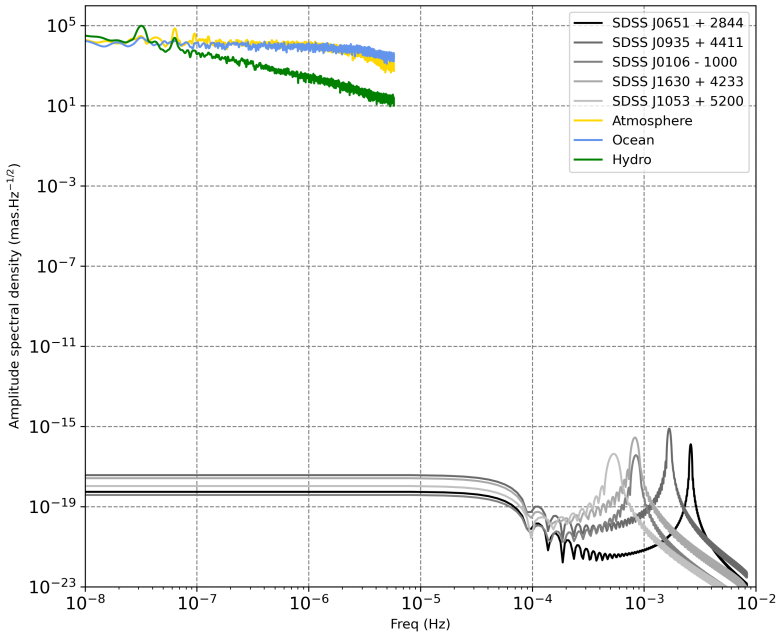

FIG. 4. Amplitude spectral density of the GW-induced polar motion variations for five different star systems during one day of observation. The GW-origin effect is compared to the effects of atmosphere, ocean and hydrology as modeled on Earth. The amplitudes of the GWs for the five star systems are between 10^{-23} and 5×10^{-22}.

In both plots, the different peaks between 0.3 and 4 mHz correspond to situations in which the GW frequency is close to, but not exactly equal to, a normal-mode eigenfrequency. True resonance would require these two frequencies to be identical. The closer the GW frequency is to the normal-mode frequency, the larger the resulting amplitude, indicating that the system is approaching resonance, at which point the amplitude would reach its maximum. This amplification by resonance is contained in the source-time functions $\bar{g}_+$ and $\bar{g}_\times$ (see appendix C), and it will affect the Earth's rotational response in the same way as for the surface ground motion ([28]). We emphasize, however, that although we study perturbations in LOD and rotation, resonance between rotational modes (as in [34]) and GW frequencies cannot occur in our framework, since we are not using the quadrupole approach (Eq. 37). Here, we consider GWs at much higher frequencies and we are computing the mass redistribution

effects after the GW has induced a relative displacement (see Eq. 2, 13, 20 and appendix C). We highlight the perturbation in the LOD associated with the five star systems and the frequencies of normal modes in Figure 5. Table III lists the frequencies of all the GWs we used and the frequencies of the gravest degree-2 modes. The frequencies related to the highest (in brown and italic) and second highest (in cyan and bold) peaks have been colorized. As expected, the highest amplification (system SDSS J0935+4111) is attributed to the system which GW frequency is the closest to a normal mode eigenfrequency.

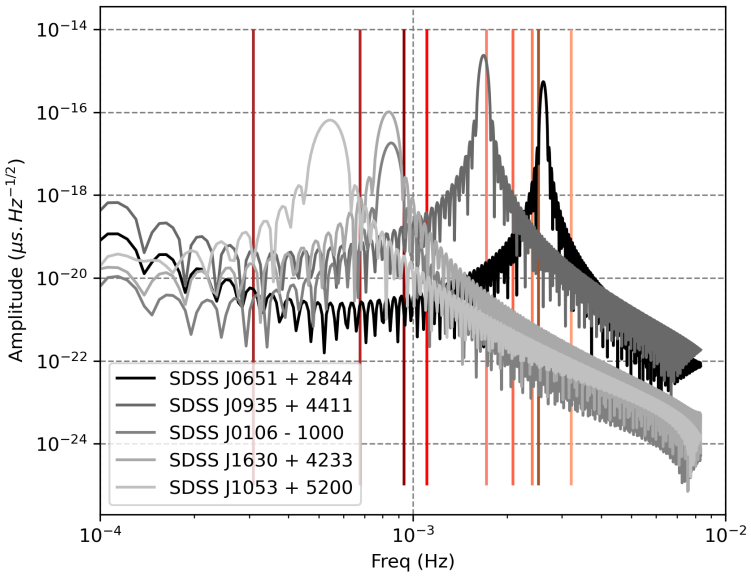

FIG. 5. Enlargement of Fig. 3 around the resonances with the degree-2 seismic modes: ${}_0S_2$: 0.309 mHz, ${}_1S_2$: 0.679 mHz, ${}_2S_2$: 0.938 mHz, ${}_3S_2$: 1.11 mHz, ${}_4S_2$: 1.72 mHz, ${}_5S_2$: 2.09 mHz, ${}_6S_2$: 2.41 mHz, ${}_7S_2$: 2.52 mHz and ${}_8S_2$: 3.21 mHz, indicated as coloured vertical lines.

Star system	f_{GW} (mHz)	Normal mode	f_{NM} (mHz)
SDSS J0651+2844	**2.613013**	${}_0S_2$	0.309
SDSS J0935+4411	*1.683502*	${}_1S_2$	0.679
SDSS J0106-1000	0.852515	${}_2S_2$	0.938
SDSS J1630+4233	0.836820	${}_3S_2$	1.11
SDSS J1053+5200	0.543478	${}_4S_2$	*1.72*
SDSS J0923+3028	0.514933	${}_5S_2$	2.09
SDSS J1436+5010	0.505433	${}_6S_2$	2.41
WD 0957-666	0.379520	${}_7S_2$	**2.52**
SDSS J0755+4906	0.367309	${}_8S_2$	3.21
SDSS J0849+0445	0.294118	${}_9S_2$	3.23
SDSS J0022-1014	0.289771	${}_{10}S_2$	4.03
SDSS J2119-0018	0.266773	${}_{11}S_2$	4.06
SDSS J1234-0228	0.253165	${}_{12}S_2$	4.33
WD 1101+364	0.159962	${}_{13}S_2$	4.84

TABLE III. Catalog of white-dwarf binaries used in this study to model GW-sources with their frequencies and compared to the frequency of the first degree-2 normal modes. White-dwarf binaries parameters were obtained from `https://www.astro.ru.nl/~nelemans/dokuwiki/doku.php?id=verification_binaries:double_white_dwarfs`

CONCLUSION

In this study, we explored the idea of using the Earth's deformability and rotation parameters as a means to detect gravitational waves (GWs). Following the approach proposed by [15], GWs were modeled as an external force acting on the Earth. We focused on the modeling of GWs emitted by white-dwarf binaries, because their signals are stable and their frequencies lie close to the frequency band of Earth's seismic normal modes.

Using a normal mode approach, we determined the surface displacement induced

by GWs ([29]). We then applied the same methodology as [18] to evaluate the GW-induced density field perturbation and rotation perturbation, an analysis that, to our knowledge, was not performed before.

The results of this first dynamic approach suggest that the GW-induced rotational and gravitational perturbations lie far below the current instrumental detection threshold. The perturbations in the LOD are around $10^{-17}\mu$s, with peaks at $10^{-15}\mu$s. These perturbations are lower than the ones modeled by [34] ($\approx 10^{-12}\mu$s in the milli-Hertz band). However, we have shown the effect of resonance with normal modes. The highest Earth's response is obtained for the white-dwarf binary system which frequency is within 0.04 mHz of the frequency of ${}_4S_2$ mode.

With the prospect of using Earth rotational perturbations as GW-detectors, it is now important to consider potential improvements to the theoretical framework employed in this study. As recently proposed by [3], Dyson's force term could be refined, which may lead to major changes in the computations proposed here. Additionally, other GW sources should be taken into account. Even though white-dwarf binaries have been chosen due to their favorable characteristics, other sources such as neutron star binary systems may lead to perturbations of higher magnitudes.

ACKNOWLEDGMENT

This work has benefited from fruitful discussions with Philippe Lognonné. We are also grateful to an anonymous reviewer which suggestions have enhanced the clarity and completeness of our study. We also thank Sophie Lambotte for providing her code to compute the splitting and coupling of modes due to the Earth's rotation and lateral heterogeneities. The eigenfunctions and eigenfrequencies of a spherically symmetric non-rotating Earth model were calculated using the MINEOS software package [42].

DATA AVAILABILITY

Observed LOD variations were downloaded from the International Earth Rotation and Reference Systems Service (IERS) (http://hpiers.obspm.fr). Atmospheric, oceanic and hydrological angular momentia were downloaded from the ESMGFZ Product Repository generated by the Earth-System-Modelling group [12]. Core angular momentum contribution was obtained from https://geodyn.univ-grenoble-alpes.fr/ [16].

APPENDIX

Appendix A: Computations

The degree-2 order-m spherical harmonic functions are written

$$Y_{2m} = \sqrt{\frac{5}{4\pi}\frac{(2-m)!}{(2+m)!}} P_{2m}(\cos\theta) e^{im\phi}, \tag{A1}$$

with the associated Legendre polynomials

$$P_{2m} = \frac{(-1)^m}{8}(1-\cos^2\theta)^{\frac{m}{2}} \frac{d^{2+m}}{d\cos\theta^{2+m}}[(\cos^2\theta - 1)^2]. \tag{A2}$$

Appendix B: Rotation matrix

Rotation matrix of the binary system from Celestial Reference Frame to Terrestrial Reference Frame is given by

$$E = \begin{bmatrix} \sin\alpha'\cos\psi - \cos\alpha'\sin\delta\sin\psi & -\sin\alpha'\sin\psi - \cos\alpha'\sin\delta\cos\psi & -\cos\alpha'\cos\delta \\ -\cos\alpha'\cos\psi - \sin\alpha'\sin\delta\sin\psi & \cos\alpha'\sin\psi - \sin\alpha'\sin\delta\cos\psi & -\sin\alpha'\cos\delta \\ \cos\delta\sin\psi & \cos\delta\cos\psi & -\sin\delta \end{bmatrix}, \tag{B1}$$

where α is the right ascension, δ the declination, and ψ the polarization angle of the binary system, and α' is defined as $\alpha - \gamma(t)$ where $\gamma(t)$ is the Greenwich Sidereal Time (GST). To express the binary system in the Terrestrial Refrence Frame we need to apply a rotation matrix E to the polarization matrices as follows

$$e_+ = \mathbf{E}\begin{bmatrix} 1 & 0 & 0 \\ 0 & -1 & 0 \\ 0 & 0 & 0 \end{bmatrix}\mathbf{E}^T \quad \text{and} \quad e_\times = \mathbf{E}\begin{bmatrix} 0 & 1 & 0 \\ 1 & 0 & 0 \\ 0 & 0 & 0 \end{bmatrix}\mathbf{E}^T. \tag{B2}$$

Appendix C: Elements of the displacement function

Source-time functions contain all the information on source frequency and rotation in time and are defined as

$$\begin{aligned}\bar{g}_+(t) &= \frac{1}{4\pi}(i\nu_k)^{-1}\frac{1}{\gamma'_k + i(2\Omega_{GW} - \omega'_k)}e^{2i\Omega_{GW}t} + \frac{1}{4\pi}(i\nu_k)^{-1}\frac{1}{\gamma'_k - i(2\Omega_{GW} + \omega'_k)}e^{-2i\Omega_{GW}t},\\ \bar{g}_\times(t) &= \frac{i}{4\pi}(i\nu_k)^{-1}\frac{1}{\gamma'_k + i(2\Omega_{GW} - \omega'_k)}e^{2i\Omega_{GW}t} + \frac{i}{4\pi}(i\nu_k)^{-1}\frac{1}{\gamma'_k - i(2\Omega_{GW} + \omega'_k)}e^{-2i\Omega_{GW}t},\end{aligned} \tag{C1}$$

where we have $\nu_k + \delta\nu_k = \omega_k + i\gamma_k + \delta\omega_k + i\delta\gamma_k = \omega'_k + \gamma'_k$ and $\Omega_{GW} = \pi f_{GW}$ is the orbital frequency of the source (f_{GW} is the GW frequency). Geometric pattern functions are defined as

$$\begin{aligned}f^m_+(\gamma(t), \alpha, \delta, \psi) &= e_+ : \frac{1}{3}I_2 = e_+ : I_1\delta_{l,2},\\ f^m_\times(\gamma(t), \alpha, \delta, \psi) &= e_\times : \frac{1}{3}I_2 = e_\times : I_1\delta_{l,2}.\end{aligned} \tag{C2}$$

with

$$\begin{aligned}I_1 = \frac{2\sqrt{\pi}}{3}\delta_{l,0}\delta_{m,0}\begin{bmatrix}1 & 0 & 0\\ 0 & 1 & 0\\ 0 & 0 & 1\end{bmatrix} + \frac{2}{3}\sqrt{\frac{\pi}{5}}\delta_{l,2}\delta_{m,0}\begin{bmatrix}-1 & 0 & 0\\ 0 & -1 & 0\\ 0 & 0 & 2\end{bmatrix}\\ + \sqrt{\frac{2\pi}{15}}\delta_{l,2}\begin{bmatrix}\delta_{m,2} + \delta_{m,-2} & i(\delta_{m,-2} - \delta_{m,2}) & \delta_{m,1} - \delta_{m,-1}\\ i(\delta_{m,-2} - \delta_{m,2}) & -\delta_{m,2} - \delta_{m,-2} & i(\delta_{m,1} + \delta_{m,-1})\\ \delta_{m,1} - \delta_{m,-1} & i(\delta_{m,1} + \delta_{m,-1}) & 0\end{bmatrix}.\end{aligned} \tag{C3}$$

These functions contain the information about the relative movement of the source and the Earth, described by the angles $\gamma(t), \alpha, \delta$, and ψ. Next, we have ζ_k, which only depends on the eigenfunctions $U_k(r), V_k(r)$ and shear modulus radial profile of the Earth ([10])

$$\zeta_k = \mu(a)a^2\big(U_k(a) + \frac{3}{\sqrt{6}}V_k(a)\big) - \int_r \frac{\partial\mu}{\partial r}\big(U_k(r) + \frac{3}{\sqrt{6}}V_k(r)\big)r^2dr. \tag{C4}$$

Finally, the eigenfunctions are renormalized to consider the Earth's rotation and ellipticity such as $\hat{s}_k(\mathbf{r}) = \mathbf{Z}^{-1}\mathbf{M}s_k(\mathbf{r})$ with

$$\begin{aligned} s_k(\mathbf{r}) &= \hat{e}_r U_k(r) Y_{2m}(\theta,\phi) \\ &+ \hat{e}_\theta \kappa^{-1} V_k(r) \partial_\theta Y_{2m}(\theta,\phi) \\ &+ \hat{e}_\phi \kappa^{-1} V_k(r) \frac{1}{\sin\theta} \partial_\phi Y_{2m}(\theta,\phi). \end{aligned} \tag{C5}$$

The Z and M matrices are obtained from the splitting matrix as defined in [10].

Appendix D: Dyadic products

$$\begin{bmatrix} \hat{e}_r \\ \hat{e}_\theta \\ \hat{e}_\phi \end{bmatrix} = \begin{bmatrix} \sin\theta\cos\phi & \sin\theta\sin\phi & \cos\theta \\ \cos\theta\cos\phi & \cos\theta\sin\phi & -\sin\theta \\ -\sin\theta & \cos\phi & 0 \end{bmatrix} \begin{bmatrix} \hat{e}_x \\ \hat{e}_y \\ \hat{e}_z \end{bmatrix} \tag{D1}$$

Hereafter we show the result of the computation of all the dyadic products in the Cartesian basis.

$$\hat{e}_r \cdot \hat{e}_r = \begin{bmatrix} \sin^2\theta\cos^2\phi & \sin^2\theta\cos\phi\sin\phi & \cos\theta\sin\theta\cos\phi \\ \sin^2\theta\cos\phi\sin\phi & \sin^2\theta\sin^2\phi & \cos\theta\sin\theta\sin\phi \\ \cos\theta\sin\theta\cos\phi & \cos\theta\sin\theta\sin\phi & \cos^2\theta \end{bmatrix} \tag{D2}$$

$$\hat{e}_r \cdot \hat{e}_\theta = \begin{bmatrix} \cos\theta\sin\theta\cos^2\phi & \cos\theta\sin\theta\cos\phi\sin\phi & -\sin^2\theta\cos\phi \\ \cos\theta\sin\theta\cos\phi\sin\phi & \cos\theta\sin\theta\sin^2\phi & -\sin^2\theta\sin\phi \\ \cos^2\theta\cos\phi & \cos^2\theta\sin\phi & -\cos\theta\sin\theta \end{bmatrix} \tag{D3}$$

$$\hat{e}_r \cdot \hat{e}_\phi = \begin{bmatrix} -\sin^2\theta\cos\phi & \sin\theta\cos^2\phi & 0 \\ -\sin^2\theta\sin\phi & \sin\theta\cos\phi\sin\phi & 0 \\ -\cos\theta\sin\theta & \cos\theta\cos\phi & 0 \end{bmatrix} \tag{D4}$$

$$\hat{e}_\theta \cdot \hat{e}_r = \begin{bmatrix} \cos\theta \sin\theta \cos^2\phi & \cos\theta \sin\theta \cos\phi \sin\phi & \cos^2\theta \cos\phi \\ \cos\theta \sin\theta \cos\phi \sin\phi & \cos\theta \sin\theta \sin^2\phi & \cos^2\theta \sin\phi \\ -\sin^2\theta \cos\phi & -\sin^2\theta \sin\phi & -\cos\theta \sin\theta \end{bmatrix} \tag{D5}$$

$$\hat{e}_\theta \cdot \hat{e}_\theta = \begin{bmatrix} \cos^2\theta \cos^2\phi & \cos^2\theta \cos\phi \sin\phi & -\cos\theta \sin\theta \cos\phi \\ \cos^2\theta \cos\phi \sin\phi & \cos^2\theta \sin^2\phi & -\cos\theta \sin\theta \sin\phi \\ -\cos\theta \sin\theta \cos\phi & -\cos\theta \sin\theta \sin\phi & \sin^2\theta \end{bmatrix} \tag{D6}$$

$$\hat{e}_\theta \cdot \hat{e}_\phi = \begin{bmatrix} -\cos\theta \sin\theta \cos\phi & \cos\theta \cos^2\phi & 0 \\ -\cos\theta \sin\theta \sin\phi & \cos\theta \cos\phi \sin\phi & 0 \\ \sin^2\theta & -\sin\theta \cos\phi & 0 \end{bmatrix} \tag{D7}$$

$$\hat{e}_\phi \cdot \hat{e}_r = \begin{bmatrix} -\sin^2\theta \cos\phi & -\sin^2\theta \sin\phi & -\cos\theta \sin\theta \\ \sin\theta \cos^2\phi & \sin\theta \cos\phi \sin\phi & \cos\theta \cos\phi \\ 0 & 0 & 0 \end{bmatrix} \tag{D8}$$

$$\hat{e}_\phi \cdot \hat{e}_\theta = \begin{bmatrix} -\cos\theta \sin\theta \cos\phi & -\cos\theta \sin\theta \sin\phi & \sin^2\theta \\ \cos\theta \cos^2\phi & \cos\theta \cos\phi \sin\phi & -\sin\theta \cos\phi \\ 0 & 0 & 0 \end{bmatrix} \tag{D9}$$

$$\hat{e}_\phi \cdot \hat{e}_\phi = \begin{bmatrix} \sin^2\theta & -\sin\theta \cos\phi & 0 \\ -\sin\theta \cos\phi & \cos^2\phi & 0 \\ 0 & 0 & 0 \end{bmatrix} \tag{D10}$$

Appendix E: Computations of integral $R_1(t)$

Hereafter we introduce the developed forms of integrals $R_1(t)$ and $R_2(t)$. The steps leading to these results are detailed in section I D.

The computation of integrals among θ and ϕ leads to the following developed form

448 of $R_{1,lm}(t)$

$$
\begin{aligned}
R_{1,lm}(t) = \int_0^a r^3 \rho(r) u_r^r(r) \Bigg(& \frac{\delta_{m,0}}{21} \begin{bmatrix} 5 & 0 & 0 \\ 0 & 5 & 0 \\ 0 & 0 & 11 \end{bmatrix} + \frac{1}{7} \begin{bmatrix} \delta_{m,1} + \delta_{m,-1} & i(\delta_{m,1} - \delta_{m,-1}) & 0 \\ i(\delta_{m,1} - \delta_{m,-1}) & \delta_{m,1} + \delta_{m,-1} & 0 \\ 0 & 0 & 0 \end{bmatrix} \\
& - \frac{1}{7}\delta_{m,0} \begin{bmatrix} 1 & 0 & 0 \\ 0 & 1 & 0 \\ 0 & 0 & 2 \end{bmatrix} + \frac{1}{28} \begin{bmatrix} -(\delta_{m,1} + \delta_{m,-1}) & i(\delta_{m,-1} - \delta_{m,1}) & 0 \\ i(\delta_{m,-1} - \delta_{m,1}) & \delta_{m,1} + \delta_{m,-1} & 0 \\ 0 & 0 & 0 \end{bmatrix} \\
& + \frac{15\pi}{128} \begin{bmatrix} 0 & i(\delta_{m,1} - \delta_{m,-1}) & 0 \\ 0 & -(\delta_{m,-1} + \delta_{m,1}) & 0 \\ 0 & 0 & 0 \end{bmatrix} \Bigg) dr \\
+\kappa^{-1} \int_0^a r^3 \rho(r) u_\theta^r(r) \Bigg(& -\frac{1}{7}\delta_{m,0} \begin{bmatrix} 1 & 0 & 0 \\ 0 & 1 & 0 \\ 0 & 0 & 2 \end{bmatrix} + \frac{1}{28} \begin{bmatrix} -(\delta_{m,1} + \delta_{m,-1}) & i(\delta_{m,-1} - \delta_{m,1}) & 0 \\ i(\delta_{m,-1} - \delta_{m,1}) & \delta_{m,1} + \delta_{m,-1} & 0 \\ 0 & 0 & 0 \end{bmatrix} \\
& + \delta_{m,0} \begin{bmatrix} \frac{45}{32}\pi & 0 & 0 \\ 0 & \frac{45}{32}\pi & 0 \\ 0 & 0 & \frac{24}{7} \end{bmatrix} + \frac{23}{56}\pi \begin{bmatrix} \delta_{m,1} + \delta_{m,-1} & i(\delta_{m,1} - \delta_{m,-1}) & 0 \\ i(\delta_{m,1} - \delta_{m,-1}) & -(\delta_{m,1} + \delta_{m,-1}) & 0 \\ 0 & 0 & 0 \end{bmatrix} \\
& + \frac{1}{8} \begin{bmatrix} 0 & \delta_{m,1} - \delta_{m,-1} & 0 \\ 0 & i(\delta_{m,1} + \delta_{m,-1}) & 0 \\ 0 & 0 & 0 \end{bmatrix} \\
& + \frac{15\pi}{128} \begin{bmatrix} 0 & 0 & 0 \\ i(\delta_{m,1} - \delta_{m,-1}) & -(\delta_{m,-1} + \delta_{m,1}) & 0 \\ 0 & 0 & 0 \end{bmatrix} \\
& + \frac{1}{8} \begin{bmatrix} 0 & 0 & 0 \\ \delta_{m,1} - \delta_{m,-1} & i(\delta_{m,1} + \delta_{m,-1}) & 0 \\ 0 & 0 & 0 \end{bmatrix} \\
& - \frac{5}{8}(\delta_{m,1} + \delta_{m,-1}) \begin{bmatrix} 0 & 0 & 0 \\ 0 & 1 & 0 \\ 0 & 0 & 0 \end{bmatrix} \Bigg) dr.
\end{aligned}
\tag{E1}
$$

Then we can extract the matrix and contraction contained into $u_r^r(r)$ and $u_\theta^r(r)$ to apply a matrix product and the contraction.

Applied for l=2, this leads to $h_{+,c}\bar{g}_+(t,\Omega,\omega_0)f^m_{I,+}(\gamma(t),\alpha,\delta,\psi)+h_{\times,c}\bar{g}_\times(t,\Omega,\omega_0)f^m_{I,\times}(\gamma(t),\alpha,\delta,\psi)$

$$
\begin{aligned}
R_{1,2m}(t) = \int_0^a r^3\rho(r)\,{}_nU_2(r)\,{}_n\zeta_2(r)\Bigg(h_{+,c}\bar{g}_+(t,\Omega,\omega_0)\Bigg[&\frac{2i}{7}\sqrt{\frac{2\pi}{15}}\delta_{m,1}e_{+,32}\\
&+\frac{2}{7}\sqrt{\frac{2\pi}{15}}\delta_{m,-1}(ie_{+,32}-e_{+,31})+\frac{4}{63}\sqrt{\frac{\pi}{5}}\delta_{m,0}\Big(-e_{+,11}-e_{+,22}+5e_{+,33}\Big)\Bigg]\\
&+h_{\times,c}\bar{g}_\times(t,\Omega,\omega_0)\Bigg[\frac{2i}{7}\sqrt{\frac{2\pi}{15}}\delta_{m,1}e_{\times,32}+\frac{2}{7}\sqrt{\frac{2\pi}{15}}\delta_{m,-1}(ie_{\times,32}-e_{\times,31})\\
&+\frac{4}{63}\sqrt{\frac{\pi}{5}}\delta_{m,0}\Big(-e_{\times,11}-e_{\times,22}+5e_{\times,33}\Big)\Bigg]\Bigg)dr\\
+\kappa^{-2}\int_0^a r^3\rho(r)\,{}_nV_2(r)\,{}_n\zeta_2(r)\Big(h_{+,c}\bar{g}_+(t,\Omega,\omega_0)\Bigg[&\frac{2}{3}\sqrt{\frac{\pi}{5}}\delta_{m,0}\Big[\frac{44}{7}e_{+,32}\\
&+(\frac{1}{7}-\frac{45\pi}{32})(e_{+,11}-e_{+,22})\Big]+\sqrt{\frac{2\pi}{15}}\delta_{m,1}\Bigg(e_{+,31}(-\frac{15\pi}{128}+\frac{i}{8})-e_{+,32}(\frac{1}{8}+\frac{15i\pi}{128}+\frac{5i}{8})\\
&+\sqrt{\frac{2\pi}{15}}\delta_{m,-1}\Big(e_{+,31}(-\frac{15\pi}{128}-\frac{i}{8})-e_{+,32}(\frac{1}{8}+\frac{15i\pi}{128}+\frac{5i}{8})\Big)\Bigg]\\
&+h_{\times,c}\bar{g}_\times(t,\Omega,\omega_0)\Bigg[\frac{2}{3}\sqrt{\frac{\pi}{5}}\delta_{m,0}\Big[\frac{44}{7}e_{\times,32}+(\frac{1}{7}-\frac{45\pi}{32})(e_{\times,11}-e_{\times,22})\Big]\\
&+\sqrt{\frac{2\pi}{15}}\delta_{m,1}\Bigg(e_{\times,31}(-\frac{15\pi}{128}+\frac{i}{8})-e_{\times,32}(\frac{1}{8}+\frac{15i\pi}{128}+\frac{5i}{8})\\
&+\sqrt{\frac{2\pi}{15}}\delta_{m,-1}\Big(e_{\times,31}(-\frac{15\pi}{128}-\frac{i}{8})-e_{\times,32}(\frac{1}{8}+\frac{15i\pi}{128}+\frac{5i}{8})\Big)\Bigg]\Bigg)dr.
\end{aligned}
\tag{E2}
$$

Here $e_{+,ij}$ or $e_{\times,ij}$ ($i\in[1;3]$) are the coefficients of matrix e_+ and $e_\times$ introduced in section I C 1.

Fully developed form of these integrals are obtained by introducing the definition of e_+ and $e_\times$ from B2.

[1] N. Ashby and J. Dreitlein. Gravitational wave reception by a sphere. Physical Review D, 12(2):336, 1975.

[2] R. T. H. Barnes, R. Hide, A. A. White, and C. A. Wilson. Atmospheric angular momentum fluctuations, length-of-day changes and polar motion. Proc R Soc Lond A, 387:31—73, 1983.

[3] E. Belgacem, M. Maggiore, and T. Moreau. Coupling elastic media to gravitational waves: an effective field theory approach. Journal of Cosmology and Astroparticle Physics, 2024. doi:10.1088/1475-7516/2024/07/028.

[4] A. Ben-Menahem. Excitation of the Earth's Eigenvibrations by Gravitational Radiation from Astrophysical Sources. II Nuovo Cimento C, 6(1):49–71, 1983.

[5] X. Bi and J. Harms. Response of the moon to gravitational waves. Phys. Rev. D, 110: 064025, Sep 2024. doi:10.1103/PhysRevD.110.064025. URL `https://link.aps.org/doi/10.1103/PhysRevD.110.064025`.

[6] W. L. Burke. On the detectability of gravitational waves from W Ursae Majoris Binary Stars. The Astrophysical Journal, 203:694–696, 1976.

[7] B. F. Chao and R. S. Gross. Changes in the Earth's rotation and low-degree gravitational field induced by earthquakes. Geophys. J. R. astr. Soc., 91:569–596, 1987.

[8] W. Chen and W. Shen. New estimates of the inertia tensor and rotation of the triaxial nonrigid earth. Journal of Geophysical Research: Solid Earth, 115(B12), 2010.

[9] M. Coughlin and J. Harms. Constraining the gravitational wave energy density of the Universe using Earth's ring. Phys. Rev. D, 90:042005, 2014.

[10] F. A. Dahlen and J. Tromp. Theoretical global seismology. Princeton University Press, 1998.

[11] A. Das, S. S. Dave, O. Ganguly, and A. M. Srivastava. Pulsars as weber gravitational wave detectors. Physics Letters B, 791:167–171, 2019. ISSN 0370-2693. doi: https://doi.org/10.1016/j.physletb.2019.02.031. URL `https://www.sciencedirect.com/science/article/pii/S0370269319301273`.

[12] H. Dobslaw and R. Dill. Predicting earth orientation changes from global forecasts of atmosphere-hydrosphere dynamics. Advances in Space Research, 61(4):1047–1054, 2018. ISSN 0273-1177. doi:https://doi.org/10.1016/j.asr.2017.11.044. URL https://www.sciencedirect.com/science/article/pii/S027311771730875X.

[13] I. M. Dozmorov. Theory of elastic solids in the gravitational internal system of reference (GISR). Soviet Physics Journal, 19(6):741–745, 1976.

[14] I. M. Dozmorov. Interaction of a gravitational wave with an elastic body. Soviet Physics Journal, 19(7):883–888, 1976.

[15] J. Dyson, F. Seismic response of the Earth to a gravitational wave in the 1-Hz band. The Astrophysical Journal, 156:529–540, 1969.

[16] D. Gillet1, N. andJault1 and C. C. Finlay. Planetary gyre, time-dependent eddies, torsional waves and equatorial jets at the earth's core surface. Journal of geophysical research: Solid Earth, 2015. doi:https://doi.org/10.1002/2014JB011786.

[17] R. Gross. 3.09 - earth rotation variations – long period. In G. Schubert, editor, Treatise on Geophysics (Second Edition), pages 215–261. Elsevier, Oxford, second edition edition, 2015. ISBN 978-0-444-53803-1. doi:https://doi.org/10.1016/B978-0-444-53802-4.00059-2. URL https://www.sciencedirect.com/science/article/pii/B9780444538024000592.

[18] R. S. Gross and B. F. Chao. The rotational and gravitational signature of the December 26, 2004 Sumatran earthquake. Surv Geophys, 27:615–632, 2006. doi:10.1007/s10712-006-9008-1.

[19] T. Hinderer. Tidal love numbers of neutron stars. The Astrophysical Journal, 677(2): 1216, apr 2008. doi:10.1086/533487. URL https://doi.org/10.1086/533487.

[20] M. Kachelrieß and M. P. Nødtvedt. Lunar response to gravitational waves. Phys. Rev. D, 110:064034, Sep 2024. doi:10.1103/PhysRevD.110.064034.

[21] H. G. Khosroshahi and Y. Sobouti. Response of a star to gravitational waves. Astronomy & Astrophysics, 321:1024–1026, 1997.

[22] J. Li, F. Liu, Y. Pan, Z. Wang, M. Cao, M. Wang, F. Zhang, J. Zhang, and Z.-H. Zhu. Detecting gravitational wave with an interferometric seismometer array on lunar

nearside. SCIENCE CHINA Physics, Mechanics & Astronomy, 66(10):109513, 2023.

[23] B. Linet. Equations Governing the Oscillations of a Self-Gravitating Elastic Sphere under the Influence of Gravitational Waves. General Relativity and Gravitation, 16(1):89–98, 1984.

[24] I. Lopes. Quadrupole stellar oscillations: The impact of gravitational waves from the Galactic Center. Physical Review D, 95:123015, 2017.

[25] I. Lopes and J. Silk. Nearby stars as gravitational wave detectors. The Astrophysical Journal, 807:1–9, 2015.

[26] I. Lopes and J. Silk. Gravitational Waves from Stellar Black Hole Binaries and the Impact on Nearby Sun-like Stars. The Astrophysical Journal, 844:1–7, 2017.

[27] M. Maggiore. Gravitational Waves, Volume 1, Theory and Experiments. Oxford University Press, 2008.

[28] J. Majstorović. Influence of gravitational waves on Earth normal modes. PhD thesis, Université de Strasbourg, 2019.

[29] J. Majstorović, S. Rosat, and Y. Rogister. Earth's spheroidal motion induced by a gravitational wave in flat space-time. Phys. Rev. D., 100, 2019. doi: 10.1103/PhysRevD.100.044048.

[30] J. Majstorović, S. Rosat, and Y. Rogister. Erratum: Earth's spheroidal motion induced by a gravitational wave in flat space-time. Phys. Rev. D., 100, 2021. doi: 10.1103/PhysRevD.100.044048.

[31] J. Majstorović, L. Vidal, and P. Lognonné. Modeling lunar response to gravitational waves using normal-mode approach and tidal forcing. Phys. Rev. D, 111:044061, Feb 2025. doi:10.1103/PhysRevD.111.044061.

[32] B. McKernan, K. E. S. Ford, B. Kocsis, and Z. Haiman. Stars as resonant absorbers of gravitational waves. Monthly Notices of the Royal Astronomical Society: Letters, 445: L74–L78, 2014.

[33] W. Munk and G. Macdonald. The Rotation of the Earth. Cambridge University Press, 1960.

[34] S. Rosat and J. Majstorović. Perturbation of the Earth's rotation by monochromatic

gravitational waves from astrophysical sources. Phys. Rev. D, 103, 2021. doi: 10.1103/PhysRevD.103.104052.

[35] D. M. Siegel and M. Roth. Excitation of non-radial stellar oscillations by gravitational waves: a first model. Monthly Notices of the Royal Astronomical Society, 408:1742–1748, 2010.

[36] D. M. Siegel and M. Roth. Excitation of stellar oscillations by gravitational waves: hydrodynamic model and numerical results from the Sun. The Astrophysical Journal, 729:1–17, 2011.

[37] F. R. Stephenson. Historical eclipses and Earth's rotation, volume 64. Cambridge University Press Cambridge, 1997.

[38] K. S. Thorne. Gravitational-wave research: Current status and future prospects. Rev. Mod. Phys., 52:285–297, Apr 1980. doi:10.1103/RevModPhys.52.285. URL `https://link.aps.org/doi/10.1103/RevModPhys.52.285`.

[39] J. M. Wahr. The effects of the atmosphere and oceans on the Earth's wobble — I. Theory. Geophysical Journal International, 70(2):349–372, 08 1982. doi:10.1111/j.1365-246X.1982.tb04972.x.

[40] R. Walgate. Gravitational waves on the Sun? Nature, 305:665, 1983.

[41] J. Weber. Detection and generation of gravitational waves. Phys. Rev., 117:306–313, 1959.

[42] J. H. Woodhouse. The calculation of eigenfrequencies and eigenfunctions of the free oscillations of the earth and the sun. In Seismological Algorithms, Computational Methods and Computer Programs, pages 321–370. D. J. Doornbos (Academic Press, London), 1988.

[43] H. Yan, X. Chen, J. Zhang, F. Zhang, M. Wang, and L. Shao. Toward a consistent calculation of the lunar response to gravitational waves. Physical Review D, 109(6): 064092, 2024.